Nanostructure and Micromechanical Properties of Reversibly Crosslinked Isotactic Polypropylene/ Clay Composites

S. Bouhelal,[1] M. E. Cagiao,[2] S. Khellaf,[1] H. Tabet,[1] B. Djellouli,[3] D. Benachour,[1] F. J. Baltá Calleja[2]

[1]*Laboratoire des Matériaux polymériques multiphasiques (LMPMP), Faculty of Engineering, Ferhat Abbas University, Sétif, Algeria*
[2]*Department of Macromolecular Physics, Instituto de Estructura de la Materia, CSIC, 28006 Madrid, Spain*
[3]*Laboratoire de génie des procédés chimiques (LGPC), Faculty of Engineering, Ferhat Abbas University, Sétif, Algeria*

Received 19 June 2008; accepted 2 November 2008
DOI 10.1002/app.29682
Published online 26 October 2009 in Wiley InterScience (www.interscience.wiley.com).

ABSTRACT: Recent developments concerning the methodology used to prepare composites of iPP and nanoclays are reported. Conventional (reactive melt mixing) and *in situ* preparations were performed, and the structural properties exhibited by the composites are discussed. Results suggest that the nanoclay could exhibit partial and, maybe, total exfoliation within the composites. Adhesion between the polymeric matrix and the nanoclay layers is similar to that obtained after grafting. The experimental procedure used and the analysis performed by means of the wide-angle X-ray scattering and differential scanning calorimetry techniques permit to describe, at nanoscale level, the contribution of the nanoclay to the polymer composite system. The microhardness values of the iPP–clay composites depend on the clay content and on the preparation method, and linearly correlate, according to the additivity law, with the degree of crystallinity. © 2009 Wiley Periodicals, Inc. J Appl Polym Sci 115: 2654–2662, 2010

Key words: nanocomposites; reactive extrusion; reversible crosslinking; polymorphism; microhardness

INTRODUCTION

The emerging nanocomposite technologies are among the most promising areas of the plastics industry to be developed during the next decades.[1] These technologies are applicable to a broad variety of polymers: polyamides and engineering thermoplastics, polycarbonates, acrylics, polyesters, polyolefins, elastomers, adhesives, and thermosetting resins. In particular, polymer–clay nanocomposites have received an increasing attention.[2–4] It is worth mentioning the outstanding contribution of Okada and Usuki in this field, both in the synthesis and development.[5] By using appropriate methods, it is possible to obtain nanocomposites with intercalated and/or exfoliated phases. This special morphology often confers peculiar characteristics to the materials, such as conductivity,[6] microporosity, enhanced gas barrier properties,[7,8] etc. These effects, usually obtained with low clay concentrations (5 wt % or less), are achieved because of the enormous interfacial adhesion region characteristics of nanocomposites. Many types of clay can be used for these preparations, montmorillonite being one of the most popular ones. It belongs to the family of so-called 2 : 1 layered or phyllosilicates. Its crystal structure consists of two tetrahedral layers of silica fused to an edge-shared octahedral sheet of either aluminum or magnesium hydroxide.[5,9] The layers stack in such a way that leave a regular Van der Waals gap between them, i.e., the interlayer space or gallery. In the pristine silicates, the interlayer spaces are usually occupied by hydrated Na^+, Ca^{2+}, or K^+ cations.[9]

In recent years, various contributions that review the different methods developed for the preparation of polymer–clay nanocomposites appeared.[5,10] One of the methods most frequently used consists in melt mixing the polymer with the clay.[4,10–14] However, to obtain a homogeneous dispersion of silicate particles in a nonpolar polymer matrix, i.e., isotactic polypropylene, iPP, is a difficult process. This is due to the fact that clay is incompatible with iPP, and the clay particles tend to agglomerate, giving rise to poorer physical properties. To avoid the agglomeration of nanoparticles, a first step that consists in premodifying the nanoclay surfaces with some organophilic agents is necessary. The resulting material is called organophilic nanoclay or organosilicate.

Correspondence to: F. J. Baltá Calleja (embalta@iem.cfmac.csic.es).

Contract grant sponsor: MEC, Spain; contract grant number: FIS2004-01331.

This process lowers the surface energy of the silicate surface, improving the wetting with the polymer matrix.[9] Thus, organosilicates are more compatible with most engineering plastics than the pristine material. The second step is to perform the melt compounding of the organosilicate either with iPP alone,[2,13] with iPP containing a small amount of functionalized monomers,[10] or with iPP and additional coupling agents, i.e., polypropylene oligomers or maleic anhydride-grafted polypropylene.[4,11,12,14] The melt compounding is made by using a polymer mixer or extruder under shear conditions. Using this method, exfoliated or intercalated polymer–clay nanocomposites can be obtained.[4,10–14] Another efficient way to break down the nanoparticle agglomerates consists in preparing the nanocomposites by means of the reactive melt mixing. Generally, a peroxide is used as the source of oxy radicals,[15] the peroxide decomposing under the appropriate processing conditions. However, this method still needs the use of clay previously organophilized.

The aims of this work are as follows:

1. To report a new approach, consisting in a rapid and easy synthesis of the new product using untreated nanoclay. Only a previous purification step is necessary (see the detailed description later). This makes the method more attractive and competitive from the industrial point of view.
2. To use the combination of peroxide, sulfur, and accelerator, which is a reactive crosslinking agent that can be used on iPP.[16–18] In this method, the reaction of the active organic part takes place outside the clay nanolayers, leading to the grafting of the polymer chains onto them.
3. To characterize the obtained composites by wide-angle X-ray scattering (WAXS) and differential scanning calorimetry (DSC).
4. To investigate the micromechanical properties of the composites and correlate them with the degree of crystallinity.

EXPERIMENTAL

Materials

The materials used in this investigation were are as follows:

- Isotactic polypropylene, iPP 05-RF03-0577 C-2807; supplied by Oriental Petrochemicals, Saudi Arabia.
- Dicumyl peroxide (DCP), 96 wt % activity; supplied by NORAX (Germany).
- Sulfur (S) (vulcanizing agent for rubber); supplied by Wuxi Huasbeng Chemical Additives Factory (China).
- Potassium persulfate; supplied by Innochem, Belgium.
- The accelerator used was "Super accelerator 501" (tetramethyl thiuram disulfide TMTD); supplied by Rhône-Poulenc, France.
- The peroxide, the sulfur, and the accelerator constitute the "crosslinking agent."
- The clay that we have used is an untreated montmorillonite called Maghnite, which was obtained from the Algerian region of Maghnia; supplied by ENOF, Algeria.

Composite preparation

We have studied a set of composites consisting of a mixture of crosslinked iPP with clay in different amounts. The clay content of the composites varies from 2 to 50 wt %. These composites have been prepared by two methods: (a) conventional and (b) *in situ*. It is noteworthy that, according to both methods, the nanoclay only needs to be previously separated from the rest of the minerals, naturally occurring metals, or impurities by washing the raw material with distilled water followed by centrifugation (no other purification process or chemical treatment of the nanoclay is necessary). Finally, the nanoclay is dried at 100°C for 24 h and screened through sieves. The preferred granular size is 63 μm or less. This granular size ensures fast miscibility and diffusion with the other components.

Conventional method

It basically consists of mixing the components (the iPP, the crosslinking agents, the potassium persulfate, and the dried and sieved nanoclay) in the corresponding weight percentage.[16–20] In the first step, the obtained compound by the crosslinking agent, the nanoclay, and potassium persulfate were mixed with the iPP in the solid state. At this stage, a small amount of vegetable oil was used to wet and facilitate the dispersion of the powder of the different components within the iPP granules. Thereafter, the so-obtained mixture was introduced into a single-screw laboratory extruder (Prolabo 1989). The extruder characteristics were as follows: $L/D = 20$; screw diameter = 25 mm; screw speed: 60 turns/min. The residence time was about 3 min. For the three stages (feed, compression, and homogenization), temperatures of 155, 180, and 200°C, respectively, were used. Composites containing 2, 4, 8, and 12 wt % of clay were prepared in one extrusion step. To prepare the composite with 16 wt % of clay, 4 wt % of clay was added to the composite with 12 wt % of clay in a second extrusion step. The same procedure was adopted to obtain composites with higher clay content (from 20 to 40 wt %). Thus, to prepare

TABLE I
iPP/Clay Composition and Preparation Method of Composites

Samples	Clay content (wt %)	Preparation method
Unmodified iPP	0	–
Crosslinked iPP	0	–
Crosslinked iPP	2	Conventional
Crosslinked iPP	4	Conventional
Crosslinked iPP	8	Conventional
Crosslinked iPP	12	Conventional
Crosslinked iPP	16	Conventional
Crosslinked iPP	20	Conventional
Crosslinked iPP	30	Conventional
Crosslinked iPP	40	Conventional
Crosslinked iPP	10	*In situ*
Crosslinked iPP	50	*In situ*

the 20 wt % composite, 4 wt % of clay was added to the 16 wt % composite in a third extrusion step, and so on. This was the only method that allowed us to incorporate up to 40 wt % of clay. The composition of the eight samples prepared by this method is shown in Table I.

In situ method

The first step is the addition of acetone to the crosslinking agent. The volume of acetone used is equal to three times the volume of the solid, taking into account that the solid is the sum of the crosslinking agent plus the clay. Then, the dried and sieved clay is added to the mixture. After few minutes, two separate phases appear, the solid phase of the functionalized clay and the liquid phase consisting of acetone plus some impurities. We also added an extra acetone quantity, just to ensure that in the upper part of the closed vessel there is only liquid. Now, after 1 day of mixing, the solid phase is ready to be blended with the iPP in the requested amount. After adding the iPP, the mixture is dried again. The drying can be performed by any conventional method, such as placing the nanocomposite in an oven for 24 h at 100°C.

The reason for thoroughly mixing the acetone, the crosslinking agent, and the clay for 1 day is to improve the penetration and diffusion of the agents between the interlayer spaces of the nanoclay. As mentioned earlier, the crosslinking agent includes the DCP and the accelerator. Both components decompose during the crosslinking reaction. However, in addition, the DCP provides the nanoclay with an ionic charge, and also swells it, creating spaces between the nanoclay layers, thus allowing the polymer chains to enter and adhere to the nanoclay layers via ionic attraction. Thus, the nanoclay is directly functionalized by means of the DCP. This means that there is an attack of the peroxide radicals on the clay nanolayers. Also, the presence of cations of different metals on the Maghnite has to be considered. In this way, an oxyreduction reaction takes place that finally grafts the macroradicals onto the clay nanolayers.

On the other hand, the acetone plays several interesting roles: (1) it enhances the dispersion of the grains before evaporation (the acetone boiling point is 56.4°C); (2) it tends to occupy the initial water spaces and absorbs the rest of the free water inside the clay; (3) the miscibility of acetone with both the peroxide and the accelerator allows a better diffusion of these agents in the interlayer clay spaces; (4) the acetone does not permit the water to be absorbed again by the functionalized clay after the preparation; for this reason, it could be considered as a conservator.

The most relevant point to be mentioned here is that by using the *in situ* method, iPP nanocomposites with clay content as high as 50 wt % have been successfully prepared in only one step. This is the most important advantage of the *in situ* method when compared with the conventional one. Only two samples prepared by this new method are included in this study (see Table I for composition). The preparation of samples with other compositions, to cover the same range as those prepared by the conventional method, is presently in progress.

For the preparation of the blends, the sulfur concentration in weight percentage was always equal to that of the peroxide. The accelerator was 1/4 of the sulfur and peroxide concentration. Finally, the weight percentage of the crosslinking agent was 1/10 of the nanoclay concentration. Table I summarizes the composition and preparation methods of the different blends.

Techniques

The samples were characterized by means of WAXS, DSC, and microindentation hardness measurements.

For the WAXS study, a Seifert diffractometer (reflection mode) was used. The following conditions were employed: 40 kV; 35 mA; angular range: 2°–35° (2θ); scan rate: 0.02°/s; slits: 0.3 and 0.2. The degree of crystallinity α_{WAXS} of all sample was derived from the ratio of the area corresponding to the crystalline peaks to the total area of the diffractogram.

The thermal analysis was performed using a Perkin-Elmer DSC-4, in an inert N_2 atmosphere. Typical sample weights were 5–10 mg. The temperature range studied was 40–200°C.

The samples were subjected to the following thermal treatment:

TABLE II
iPP/Clay Composites

Clay content	T_m^α (°C)	l_c^α (nm)	T_m^β (°C)	l_c^β (nm)	ΔH_m (J/g)	α_{DSC}	α_{WAXS}	H (MPa)
Unmodified iPP	159.6	16.7	–	–	96.4	0.47	0.47	85
0	161.7	18.1	–	–	99.2	0.48	0.55	92
2	158.9	16.3	–	–	88.0	0.42	0.47	100
4	150.7	12.7	–	–	81.2	0.40	0.45	68
8	159.2	16.5	–	–	82.6	0.40	0.47	96
12	160.5	17.3	–	–	89.8	0.43	0.51	103
16	158.5	16.1	145.2	18.2	87.3	0.43	0.51	89
20	159.4	16.6	145.4	18.3	82.9	0.41	0.53	88
30	159.9	16.9	146.2	18.7	75.0	0.37	0.46	83
40	159.0	16.4	142.5	16.9	78.8	0.38	0.48	86
10	161.4	17.9	–	–	88.6	0.43	0.49	94
50	159.1	16.4	145.5	18.3	84.3	0.41	0.43	102

Melting points, T_m^α and T_m^β from DSC; crystal thickness values, l_c^α and l_c^β derived from the melting points; total melting enthalpy ΔH_m; crystallinity values α_{DSC} and α_{WAXS} and microhardness H.

1. Heating from 40 up to 200°C, at 20°C/min.
2. Fast cooling down to 40°C.
3. Heating from 40 to 200°C, at 10°C/min.
4. Five minutes at 200°C.
5. Slow cooling down from 200 to 40°C, at 5°C/min.

The crystal thickness corresponding to the different melting peaks appearing in the thermograms were estimated using the Thomson-Gibbs equation[21]:

$$T_m = T_m^0[1 - (2\sigma_e/\Delta H_m^\infty l_c)] \quad (1)$$

where σ_e is the surface free energy, T_m^0 is the equilibrium melting point of each component, and ΔH_m^∞ is the melting enthalpy for an infinitely thick crystal.

Microhardness, H, was determined at room temperature using a Leitz microindentation tester, adapted with a square-based diamond indenter.[22] The H-value was derived from the residual projected area of indentation according to the expression: $H = kP/d^2$, where d is the length of the impression diagonal in meters, P is the contact load applied in N, and k is a geometrical factor equal to 1.854. Loads of 0.25, 0.5, and 1 N were used. The loading cycle was 0.1 min. The hardness measurements were averaged over 8–10 indentations on each sample.

RESULTS

The melting point, crystal thickness, melting enthalpy, degree of crystallinity, and microhardness values for the crosslinked iPP/clay samples are listed in Table II.

Wide-angle X-ray scattering

Figure 1(a) and (b) shows the diffractograms of the blends of iPP with 8 and 10 wt % of clay, respectively. The first composition was prepared by the conventional method, and the second one by the *in situ* method. The X-ray diffraction pattern of all the clay-containing samples (except the one with a 4 wt % of clay) exhibits, besides the typical reflections of the α-form of iPP,[23] two additional peaks at 6.9° and 26.7° (2θ); the first one is characteristic of the d_{001} spacing of clay; the second one, much less intense, is ascribed to the quartz that usually accompanies the clay. On the other hand, in almost all the crosslinked iPP samples, two maxima at 16.2° and 20.1° (2θ) appear. The first reflection corresponds to the β crystalline modification of iPP,[23] and the second one to the γ-form.[23] The γ-form is already present in the diffractogram of the crosslinked sample with no clay (data not shown here). However, in the sample with 12 wt % of clay and in the two samples prepared by the *in situ* method, only the reflection at 20.1° (2θ) (γ-form)[23] appears [compare, for instance, Fig. 1(a,b)]. In Figure 1, the reflections corresponding to the clay, the quartz, and the β- and γ-forms of iPP are indicated by small arrows.

In all the crosslinked samples, the intensity of the second reflection (at about 16.7° of 2θ) is higher than that of nonmodified iPP. This could be explained by the appearance of the γ-form in the modified material (both α and γ crystalline forms show a reflection in this position).[23] In addition, in the sample with a 20 wt % of clay, the contribution to the β-form reaches the highest value, representing ~8% of the total diffracted intensity or 13% over the crystalline material.

The α_{WAXS} values are also listed in Table II. This table also includes the values found on the unmodified iPP. Figure 2 illustrates the variation of the degree of crystallinity α_{WAXS} (after subtraction of the clay and quartz contribution) as a function of clay content. It shows, in addition, the scattered intensity of the clay maximum [at about 6.9° (2θ)] to the WAXS patterns for the different compositions.

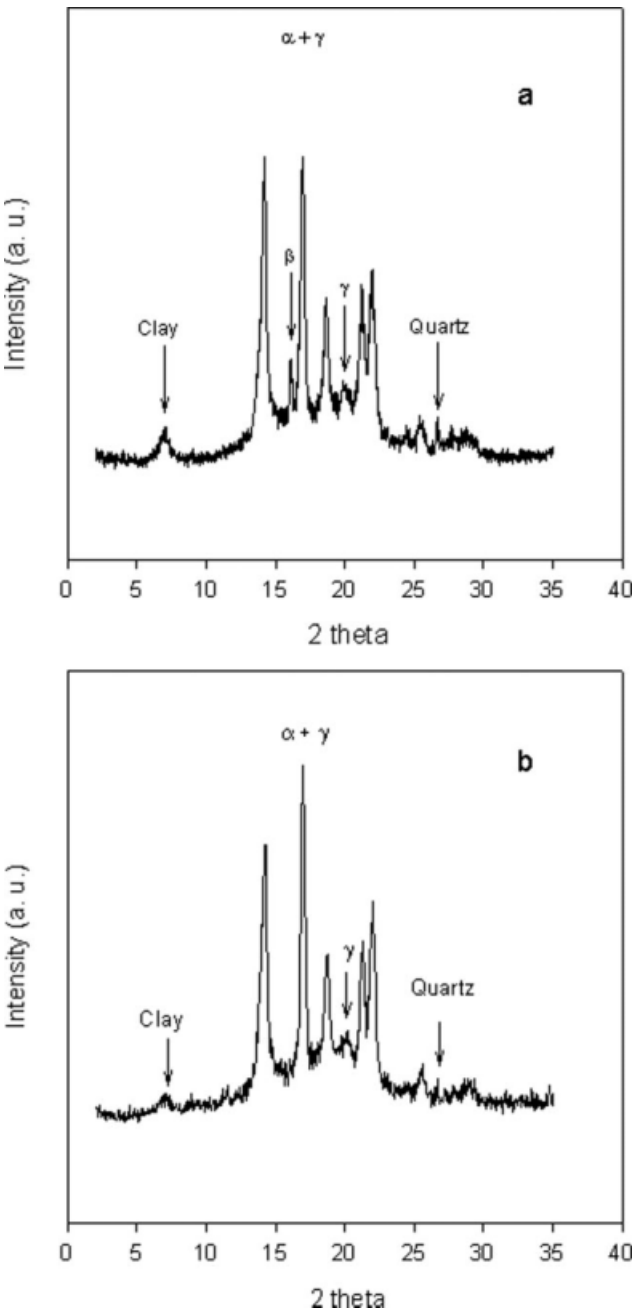

Figure 1 Diffractograms of crosslinked iPP nanocomposites with (a) 8 wt % and (b) 10 wt % of clay. The first composite was prepared by the conventional method, and the second one by the *in situ* method.

Differential scanning calorimetry

The first run of the thermograms for all samples [see Fig. 3(a)] shows one melting peak that corresponds to the α-form of the iPP. In samples with clay content equal or higher than 16 wt %, a lower temperature melting peak also appears. This low temperature peak is related to the β-form of iPP. The thermograms obtained in the second run [see Fig. 3(b)] are similar to those shown in the first heating, although they are more complex. Here, the main melting peak appears at temperatures 3–4°C lower than in the first run. The sample with 4 wt % of clay does not seem to show any difference between the first and second heating. In the thermograms obtained during the cooling process (data not shown here), only one crystallization peak appears at a temperature about 20°C lower that the corresponding to the main melting peak. In all the crosslinked samples, even the one with no clay, the crystallization temperature exceeds from 7 to 12°C the corresponding to the unmodified iPP.

From the thermograms, we have calculated the total degree of crystallinity, α_{DSC}, and the crystal thickness l_c^α derived from the position of the main melting peak T_m^α (Table II). Table II also lists the second melting peak T_m^β found for the compositions with clay content from 16 wt % onward, together with their corresponding crystal thickness l_c^β. We have used the following values for these calculations: (a) for the α-form of iPP, we have taken $\Delta H_m^\infty = 207.33$ J/g,[21] $T_m^0 = 460.7$ K,[21] and $\sigma_e = 100$ erg/cm^2 (Ref. 24); (b) for the β-form, we have used $\Delta H_m^\infty = 168.5$ J/g,[25] $T_m^0 = 456$ K,[26] and $\sigma_e = 119$ erg/cm^2.[27]

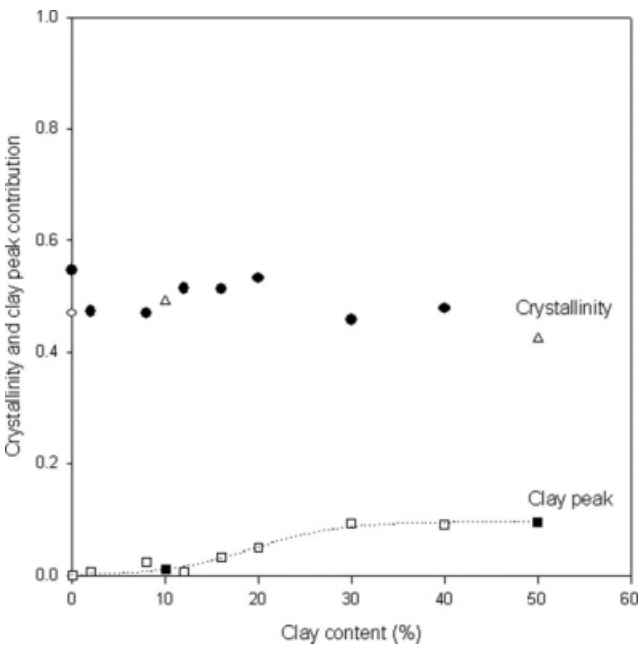

Figure 2 WAXS crystallinity and clay peak contribution of the crosslinked iPP/clay nanocomposites as a function of the clay content. Symbols are as follows: Crystallinity: (○) noncrosslinked iPP sample; (●) blends iPP/clay prepared by the conventional method; (Δ) blends iPP/clay prepared by the *in situ* method. Clay peak contribution: (□) blends iPP/clay prepared by the conventional method; (■) blends iPP/clay prepared by the *in situ* method.

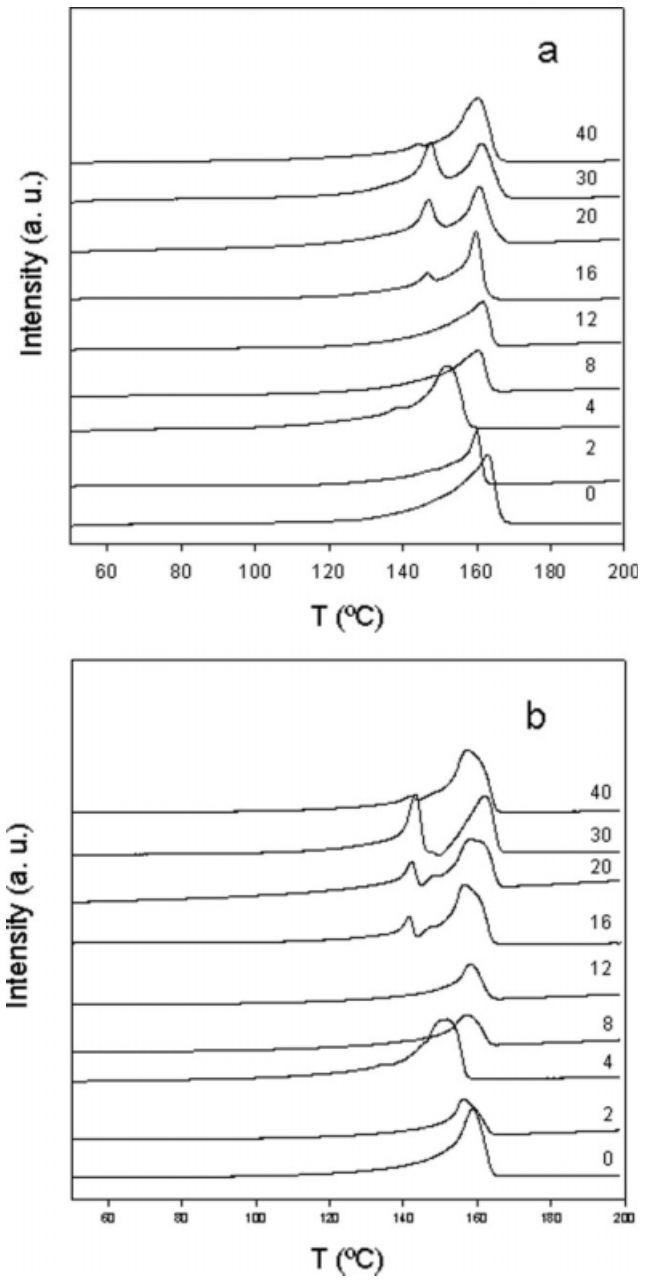

Figure 3 DSC thermograms of the crosslinked iPP–clay nanocomposites: (a) first heating run and (b) second heating run. Clay content is indicated on each curve.

Microhardness

The variation of microhardness H with clay content is illustrated in Figure 4. A slight depression of the H values for the compositions ranging from 16 to 40 wt % of clay is clearly visible here. The H values of all the samples are also collected in Table II. From this table, it can be seen that the composite with 4 wt % of clay, not included in Figure 4, shows a H value notably lower than those exhibited by the rest of compositions.

DISCUSSION

Dependence of crystallinity on clay content

As mentioned earlier, the diffractograms of almost all the clay-containing samples show two characteristics reflections at 6.9° and 26.7° (2θ). The first one, that is characteristic of clay, is the most intense. The second one is related to the quartz that usually appears together with the clay. The diffractogram of the dry clay, not shown here, exhibits the first maximum (001 planes) at 6.23° (2θ). This means that, in the blends with iPP, the corresponding clay spacing becomes smaller. As it was indicated earlier, Figure 2 shows the crystallinity α_{WAXS} dependence on the clay content for all the samples investigated. These data have been obtained from the WAXS patterns of the samples, after subtraction of the clay and quartz contribution. It is noteworthy that samples with a clay content of 10 and 50 wt %, which were prepared by a different method, i.e., *in situ* method, fit well in the plot. It can be seen that α_{WAXS} slowly decreases for samples with clay content higher than 20%. This effect can be explained by the presence of increasing amounts of clay, which can restrict the growing rate and therefore the mobility of the iPP chains. On the other hand, the clay also is a nucleating agent and enhances the iPP nucleation rate. Hence, its crystallization capability will be restricted.

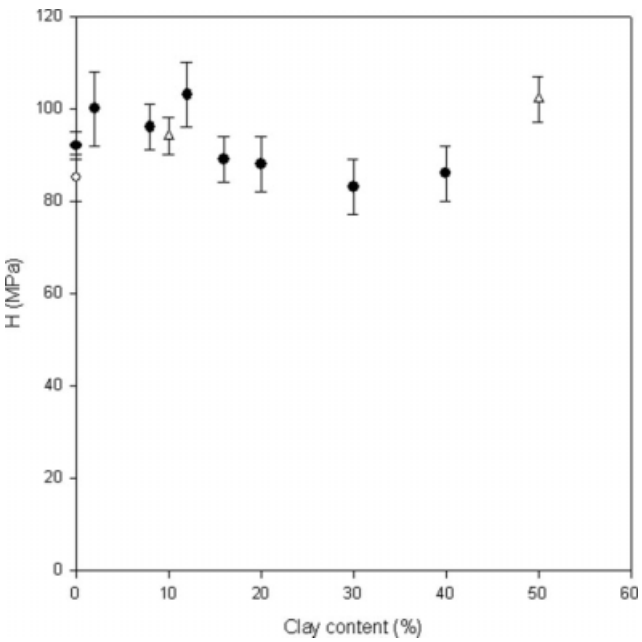

Figure 4 Hardness dependence of the crosslinked iPP–clay nanocomposites on the clay content. Symbols are as follows: (○) noncrosslinked iPP sample; (●) blends iPP/clay prepared by the conventional method; (Δ) blends iPP/clay prepared by the *in situ* method.

Figure 2 (bottom) also shows the contribution of the clay peak to the total diffracted intensity as a function of clay content. For samples containing up to 12 wt % clay, this contribution is very small (lower than 2%), slowly increasing until 9.5% for clay content equal or higher than 30 wt %. This could be an indication that, for the majority of compositions studied, a certain intercalation or a partial exfoliation of clay may be achieved. Nevertheless, the fact that the (001) clay peak appears in nanocomposites at higher scattering angles than in the pristine clay suggests that the corresponding *d*-spacing is smaller. In addition, a fraction more or less important of the original clay particles remains unmodified.[12]

In Table II, it is seen that the blend with 4 wt % of clay, not included in the plots, shows minimum values for α_{WAXS}, α_{DSC}, and H. In addition, the first and second thermograms obtained on this sample [see Fig. 3(a,b)] are practically identical. Moreover, as mentioned earlier, the diffractogram of this composition does not show any clay or quartz reflections. This could be due to the fact that, for this composition, a nanocomposite structure is obtained, i.e., a complete exfoliation process of the clay has occurred. However, this assumption should be supported by SAXS experiments and/or AFM observations.[13] In fact, it is known that extensive intercalation could separate clay layers to such an extent that WAXS could not detect them, but still they could be detected by SAXS and TEM.[28] We are preparing the SAXS and/or AFM study of some blends to clarify this aspect.

Polymorphism

The crystallinity values α_{DSC}, derived from the thermograms of the different compositions studied are listed in Table II. They are lower than the α_{WAXS} obtained from the crystallographic study, differences being between 2 and 10% as a maximum.

As it was mentioned earlier, the low-temperature melting peak appearing in the thermograms of some compositions, in particular, those with 16, 20, 30, and 40 wt % of clay [see Fig. 3(a,b)] is due to the contribution of the β-form. As indicated in the preceding section, β- and γ-forms appear in the X-ray diffraction patterns of almost all the crosslinked iPP/clay samples. However, the amount of the β-form (calculated from the WAXS patterns) in samples with clay content below 16% is very small (less than 1% of the total diffracted intensity). Probably for this reason, it cannot be detected in the thermograms. Furthermore, the lower melting peak intensity gradually increases when passing from the sample with a clay content of 16 wt % to the one with 30 wt %, its contribution being small again in the sample with a 40 wt % of clay. The observation of the second T_m^β in the composites ranging from 16 wt % up to 40 wt % of clay is related to the fact that, as indicated in the "Experimental" section under "Conventional method," these samples were subjected to repeated extrusion cycles, thus having experienced a more intense shearing. Such a high shearing is responsible for the partial exfoliation of the nanoclay remaining in each repeated cycle, and also, for the appearance of the β-crystalline form in higher amounts. According to Marigo et al.[29] and Moitzi and Skalicky,[30] it is to be noted that, when molten iPP is subjected to shear, the formation of the β-type crystals is favored. On the other hand, the repeated extrusion cycles do not significantly change the properties of the material. This is in favor of the reversibility of the process used to prepare the crosslinked iPP/clay samples.

The polymorphism shown by the samples with clay content between 16 and 40 wt % is more pronounced in the second run [Fig. 3(b)]. In fact, according to preceding data,[29,30] for a clay content of 16 or 20 wt %, the first two peaks are related to the melting of the original β_1-form that recrystallizes, during the heating process, in the more stable β_2-form, and its melting. Moreover, the third endotherm is related with the melting of the original α-crystals and the ones recrystallized after the melting of β_2.[29,31] The reason for not having found these separate effects in the first run is that both runs have been performed at different heating rates, i.e., 20 and 10°C/min, respectively, and it has been demonstrated[29,31] that the amount of the $\beta_1-\beta_2$ recrystallization decreases and the intensity of the β melting endotherm[29] increases when the heating rate increases. In addition, at the lower heating rate (10°C/min), a shoulder in the higher temperature region can be observed, indicative of the double melting behavior of the α-form.[29,32]

Correlation of microhardness and level of crystallinity

The depression of the hardness values found in samples from 16 to 40 wt % of clay [see Fig. 4] could be explained by a combination of several effects: (a) the lower crystallinities shown by these samples when compared with the rest of compositions [see Fig. 2 and Table II]; (b) the coexistence for these compositions of two crystalline forms with two average lamellar thicknesses; and (c) the influence that the repeated extrusion cycles may have on the surface free energy σ_e value of the crystals.

As it is known, the hardness H of a polymer can be expressed in terms of its crystalline H_c and amorphous H_a components, according to the additivity law[33]:

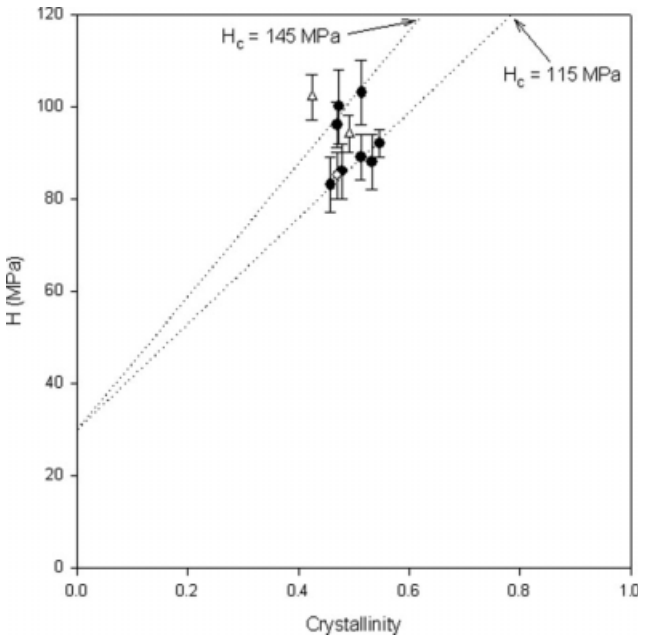

Figure 5 Hardness–crystallinity relationship on crosslinked iPP–clay nanocomposites. Symbols are as indicated in Figure 4.

$$H = H_c\alpha + H_a(1 - \alpha) \quad (2)$$

where α stands for the degree of crystallinity of the polymer. On the other hand, the crystal hardness H_c is related to the crystal thickness l_c through the expression[34]:

$$H_c = H_c^{\infty}/(1 + b/l_c) \quad (3)$$

in which H_c^{∞} is the hardness of an infinitely thick crystal, and the b-parameter is defined as: $b = 2\sigma_e/\Delta h$,[34] σ_e being the free surface energy and Δh is the energy required for the plastic deformation of the crystals. The data of Table II show that the thickness of the β-crystals is slightly higher than that of the α-crystals. Nevertheless, the crystalline hardness corresponding to the β-form is lower than the one exhibited by the α-crystals, $H_c^{\alpha} = 143$ MPa and $H_c^{\beta} = 119$ MPa.[27] In any case, the β-crystals represent, as a maximum, only a 13% of the crystalline material in the sample with a 20 wt % of clay. This means that the influence of the β-crystals on the H value is not enough as to take it into account in the hardness depression. On the other hand, the σ_e value is a measure of the degree of order at the crystals surface, which is in turn affected by the blending process.[35] Thus, the decrease in hardness for samples with 16 to 40 wt % of clay is thought to be mainly related with the diminution of crystallinity shown by these compositions and also with the increase in the σ_e value originated by the repeated extrusion cycles necessary to prepare the samples with higher clay contents. Evidently, this last effect is directly related to the selected preparation method.

This behavior is also illustrated in Figure 5, which shows the relationship between the hardness H and the WAXS crystallinity for all the composites. Taking into account that the amorphous hardness of iPP is $H_a = 30$ MPa,[36] in Figure 5, two straight lines can be drawn that encompass all our experimental data (except the sample with 50 wt % of clay). From the additivity law [eq. (2)], two H_c values can be derived for the two straight lines, i.e., 145 and 115 MPa. It is interesting to note that the samples with higher H_c values (or lower surface free energy, σ_e) are those that have been extruded only once (see Conventional method under Experimental section). On the contrary, most of the samples that show lower H_c (or higher σ_e values) have been extruded several times.

CONCLUSIONS

1. Composites of reversibly crosslinked iPP with increasing amounts of nanoclay have been prepared by two different methods, conventional and *in situ*. These methods involve the use of a simple procedure to purify the nanoclay before preparing the composites.
2. By using the *in situ* method, both the crosslinking iPP process and the composite preparation are performed in only one step. This method allows the preparation of nanocomposites with clay content as high as 50 wt %, i.e., notably higher than the obtained by the conventional method.
3. Following both methods and depending on the clay concentration, partial or even, total exfoliation of clay may be assumed. However, this point requires further verification.
4. Any kind of industrial equipments can be used to perform the reactive melt processing, i.e., injection molding, calendering, etc. In each processing method, the effective shearing produced on the composites is different.
5. All the crosslinked samples show polymorphism. The β-form and its transformations during the heating process are responsible for the melting behavior of the samples with 16 to 30 wt % of clay.
6. The nanoclay content seems to affect the nanostructure and consequently the microhardness of the samples in a quite similar way.
7. Results reveal that the microhardness of the samples is also affected by the preparation method, influencing the surface free energy of the crystals.

References

1. Meyers, M. A.; Ritchie, R. O.; Sariyaka, M., Eds. Nano and Microstructural Design of Advanced Materials; Elsevier: Oxford, 2003.
2. Yuan, Q.; Awate, S.; Misra, R. D. K. Eur Polym J 2006, 42, 1994.
3. Gelfer, M.; Burger, C.; Fadeev, A.; Sics, I.; Chu, B.; Hsiao, B. S.; Heintz, A.; Kojo, K.; Hsu, S.-L.; Si, M.; Rafailovich, M. Langmuir 2004, 20, 3746.
4. Kiersnowski, A.; Chamczynska, J.; Trelinska-Wlazlak, M.; Lesniewicz, A.; Pigloswki, J. e-Polymers 2005, P_008, 1 (Conference paper, International Polymer Seminar, Gliwice-Poland, 2005).
5. Okada, A.; Usuki, A. Macromol Mater Eng 2006, 291, 1449.
6. Kurian, M.; Galvin, M. E.; Trapa, P. E.; Sadoway, D. R.; Mayes, A. M. Electrochim Acta 2005, 50, 2125.
7. Vladimirov, V.; Betchev, C.; Vassiliou, A.; Papageorgiu, G.; Bikiaris, D. Compos Sci Technol 2006, 66, 2935.
8. Frounchi, M.; Dadbin, S.; Salehpour, Z.; Noferesti, M. J Membr Sci 2006, 282, 142.
9. Giannelis, E. P. Adv Mater 1996, 8, 29.
10. Manias, E.; Touny, A.; Wu, L.; Strawhecker, K.; Lu, B.; Chung, T. C. Chem Mater 2001, 13, 3516.
11. Reichert, P.; Nitz, H.; Klinke, S.; Brandtsch, R.; Thomann, R.; Mülhaupt, R. Macromol Mater Eng 2000, 275, 8.
12. Rohlmann, C. O.; Failla, M. D.; Quinzani, L. M. Polymer 2006, 47, 7795.
13. Ramos Filho, F. G.; Mélo, T. J. A.; Rabello, M. S.; Silva, S. M. L. Polym Degrad Stab 2005, 89, 383.
14. Sirousazar, M.; Yari, M.; Achachlouel, B. F.; Arsalani, J.; Mansoori, Y. e-Polymers 2007, 027.
15. Shi, D.; Hu, G.-H.; Li, R. K. Y. J Chem Eng Sci 2006, 61, 3780.
16. Bouhelal, S. U.S. Pat. 6,987,149 (2006).
17. Bouhelal, S. U.S. Pat. 7,241,844, (2007).
18. Bouhelal, S. U.S. Pat. 7,309,744, (2007).
19. Bouhelal, S.; Cagiao, M. E.; Benachour, D.; Baltá Calleja, F. J. J Appl Polym Sci 2007, 103, 2968.
20. Bouhelal, S.; Cagiao, M. E.; Khellaf, S.; Benachour, D.; Baltá Calleja, F. J. J Appl Polym Sci 2008, 109, 795.
21. Wunderlich, B. Macromolecular Physics; Academic Press: New York, 1980; Vol. 3: Crystal Melting, p. 48.
22. Baltá Calleja, F. J.; Fakirov, S. Microhardness of Polymers (Solid State Science Series); Cambridge University Press: Cambridge, 2000.; Chapter 1, p 3 and Chapter 2, p 16.
23. Karger-Kocsis, J., Ed. Polypropylene; Chapman and Hall: London, Vol. 1, 1995.
24. Flores, A.; Aurrekoechea, J.; Gensler, R.; Kausch, H. H.; Baltá Calleja, F. J. Colloid Polym Sci 1998, 276, 786.
25. Li, J. X.; Cheung, W. L.; Jia, D. Polymer 1999, 40, 1219.
26. Varga, J. J Therm Anal 1986, 31, 165.
27. Baltá Calleja, F. J.; Martínez Salazar, J.; Asano, T. J Mater Sci Lett 1988, 7, 165.
28. Benetti, E. M.; Causin, V.; Marega, C.; Marigo, A.; Ferrara, G.; Ferraro, A.; Consalvi, M.; Fantinel, F. Polymer 2005, 46, 8275.
29. Marigo, A.; Marega, C.; Causin, V.; Ferrari, P. J Appl Polym Sci 2004, 91, 1008.
30. Moitzi, J.; Skalicky, P. Polymer 1993, 34, 3168.
31. Shi, G.; Zhang, X.; Cao, Y.; Hong, J. Makromol Chem 1993, 194, 269.
32. Guerra, G.; Petraccone, V.; Corradini, P.; De Rose, C.; Napolitano, R.; Pirozzi, B.; Giunchi, G. J Polym Sci Polym Phys Ed 1984, 22, 1029.
33. Baltá Calleja, F. J.; Fakirov, S. Microhardness of Polymers (Solid State Science Series); Cambridge University Press: Cambridge, 2000; Chapter 4, p. 91.
34. Baltá Calleja, F. J.; Fakirov, S. Microhardness of Polymers (Solid State Science Series); Cambridge University Press: Cambridge, 2000; Chapter 4, p. 95.
35. Baltá Calleja, F. J.; Fakirov, S. Microhardness of Polymers (Solid State Science Series); Cambridge University Press: Cambridge, 2000; Chapter 7, p. 205.
36. Martínez Salazar, J.; García Tijero, J. M.; Baltá Calleja, F. J. J Mater Sci 1988, 23, 862.